In-plane anisotropy of the optical and electrical properties of layered ReS_2 crystals

1999 J. Phys.: Condens. Matter 11 5367

(http://iopscience.iop.org/0953-8984/11/27/312)

J. Phys.: Condens. Matter **11** (1999) 5367–5375. Printed in the UK PII: S0953-8984(99)01701-4

In-plane anisotropy of the optical and electrical properties of layered ReS_2 crystals

C H Ho†‖, Y S Huang†¶, K K Tiong‡ and P C Liao§

† Department of Electronic Engineering, National Taiwan University of Science and Technology, Taipei 106, Taiwan, Republic of China
‡ Department of Electrical Engineering, National Taiwan Ocean University, Keelung 202, Taiwan, Republic of China
§ Department of Electronic Engineering, Kuang Wu Institute of Technology and Commerce, Peitou 112, Taiwan, Republic of China

Received 9 February 1999

Abstract. In-plane anisotropic optical and electrical properties of layered ReS_2 crystals are reported. The optical anisotropic effects for $\boldsymbol{E} \parallel \boldsymbol{b}$ polarization and $\boldsymbol{E} \perp \boldsymbol{b}$ polarization were studied through polarization-dependent piezoreflectance and optical absorption measurements. The resistivity perpendicular to the *b*-axis was shown to be several times larger than that along the *b*-axis.

1. Introduction

ReS_2 is a diamagnetic semiconductor that belongs to the family of the layered-type transition-metal dichalcogenides [1, 2]. The properties of the transition-metal dichalcogenides have been reviewed by Wilson and Yoffe [1]. The layered-type transition-metal dichalcogenides crystallize in a lattice with strong covalent bonds within a layer and weak interactions, usually of the van der Waals type, between the individual layers. The strong anisotropy in the chemical bonds leads to anisotropy in many material properties parallel and perpendicular to the layers [3]. Unlike most of the layered transition-metal dichalcogenides, ReS_2 has a distorted $CdCl_2$ structure, leading to triclinic symmetry [2, 4]. Crystals with triclinic symmetry are optically biaxial. Therefore, an anisotropic response of ReS_2 is expected for linearly polarized light, incident normal to the basal plane ($\boldsymbol{E} \parallel (001), \boldsymbol{k} \perp (001)$). This behaviour differs from that of transition-metal dichalcogenides with hexagonal structure (e.g., 2H-MoS_2), which are optically uniaxial with the optical axis perpendicular to the van der Waals plane. Wilson and Yoffe claimed biaxial behaviour for ReS_2. However, to date, no detailed anisotropic optical and electrical properties in the van der Waals plane have been reported. To the best of our knowledge, only Friemelt *et al* [5], in a recent article, have reported anisotropic effects in the van der Waals plane of ReS_2 single crystals and mentioned that ReS_2 may be of interest for fabrication of polarization-sensitive photodetectors in the visible wavelength region.

In this paper we report a detailed study of the in-plane anisotropic optical and electrical properties of ReS_2 single crystals. The direct band-edge excitonic transitions and indirect

‖ Present address: Department of Electronic Engineering, Kuang Wu Institute of Technology and Commerce, Peitou 112, Taiwan, Republic of China.
¶ Author to whom any correspondence should be addressed.

0953-8984/99/275367+09$30.00

band-edge transitions are studied by polarization-dependent piezoreflectance (PzR) and transmittance, respectively, at 25 and 300 K. In addition, temperature-dependent resistivity measurements along and perpendicular to the *b*-axis were also carried out in the temperature range from 80 to 300 K. The resistivity perpendicular to the *b*-axis was shown to be much larger than that along the *b*-axis.

2. Experimental procedure

Single crystals of ReS_2 were grown by the chemical vapour transport method, using Br_2 as a transport agent, leading to n-type conductivity. Prior to the crystal growth, quartz tubes containing Br_2 and the elements (Re: 99.95% pure, S: 99.999%) were evacuated and sealed. The quartz tube was placed in a three-zone furnace and the charge prereacted for 24 h at 800 °C with the growth zone at 1000 °C, preventing transport of the product. The furnace was then equilibrated to give a constant temperature across the reaction tube and was programmed over 24 h to produce the temperature gradient at which single crystal growth takes place. The best results were obtained with temperature gradients of 1060 °C → 1000 °C. Single crystals of ReS_2 formed thin, silver-coloured, graphite-like platelets up to 2 cm^2 in area and 100 μm in thickness. X-ray diffraction patterns confirmed the triclinic symmetry of ReS_2 with all parameters consistent with those previously reported [2]. The weak van der Waals bonding between the layers of the material has the result that they display good cleavage parallel to the layers, which can be exploited to obtain thin specimens.

Measurements of the reflectance and transmittance at near-normal incidence were made on a Bruker model IFS 120 HR in the range 8000–13 500 cm^{-1}, with a resolution of 4 cm^{-1}. The transmission intensity was closely monitored to maintain an incidence close to 90°. Single crystals with a thickness of about 10 μm were used for the transmittance measurements. Plate-shaped crystals were selected and mounted on a copper sample holder fitted into a Dewar with optical windows. The PzR measurements were achieved by gluing the thin single-crystal specimens on a lead zirconate titanate (PZT) piezoelectric transducer, 0.15 cm thick, driven by a 200 V_{rms} sinusoidal wave at 200 Hz. The alternating expansion and contraction of the transducer subjects the sample to an alternating strain with a typical rms $\Delta l/l$ value of $\sim 10^{-5}$. An 150 W tungsten–halogen lamp filtered by a model 270 McPherson 0.35 m monochromator provided the monochromatic light. The reflected light was detected by an EG&G type HUV-2000B silicon photodiode, and the signal was recorded from an NF 5610B lock-in amplifier. An RMC model 22 closed-cycle cryogenic refrigerator equipped with a model 4075 digital thermometer controller was used for the low-temperature measurements. Oriel near-infrared dichroic sheet polarizers were employed for the polarization-dependent measurements.

The temperature dependence of the resistivity was studied between 80 and 300 K by using a four-probe potentiometric technique. The selected sample was cut into a rectangular shape. Electrical connections to the crystal were made by means of four parallel gold wires (parallel or perpendicular to the *b*-axis) laid across the basal surface of the thin crystal and attached to the crystal surface by means of conducting silver paint. The wires near each end of the rectangular crystal acted as current leads, while the two contact wires on either side of the central line were used to measure the potential difference V in the crystal. The potential difference V measured by a sensitive potentiometer is taken to be the average value obtained on reversing the current through the sample. Shown in figure 1 are the crystal morphology and the crystal structure in the van der Waals plane of ReS_2; the as-grown thin dark lines in the crystal plane correspond to the orientation of the *b*-axis. The *b*- and *a*-axes are the shortest and second-shortest axes in the basal plane; the *b*-axis is parallel to the Re-cluster chains and corresponds to the longest edge of the plate.

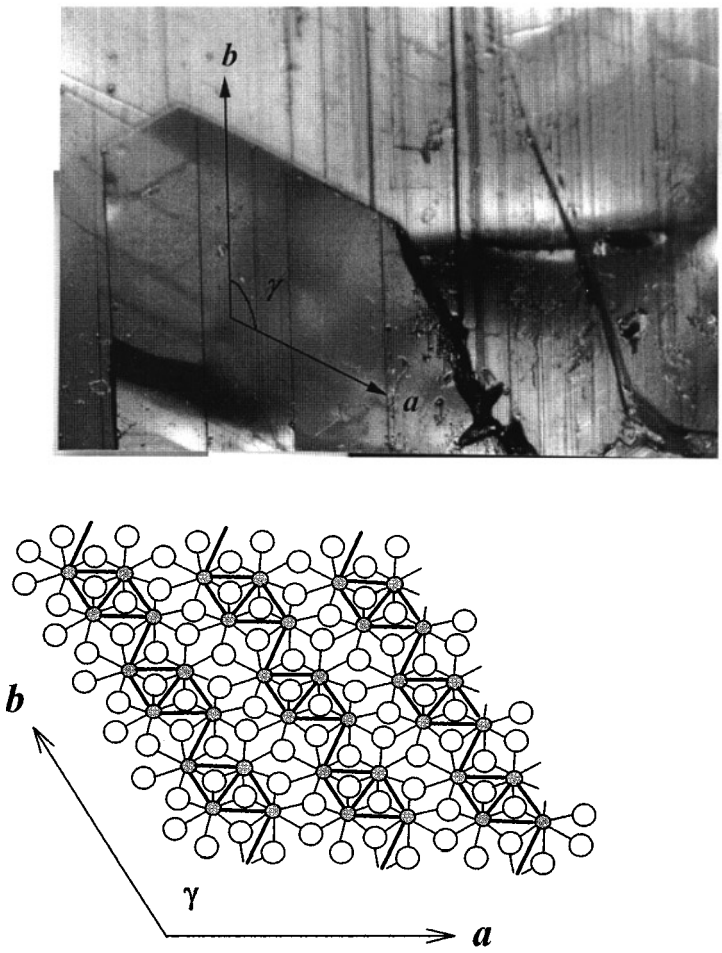

Figure 1. The crystal morphology and crystal structure in the van der Waals plane of ReS_2 single crystals. The as-grown thin dark lines in the crystal plane correspond to the orientation of the *b*-axis.

3. Results and discussion

The unpolarized, $\boldsymbol{E} \parallel \boldsymbol{b}$ polarization and $\boldsymbol{E} \perp \boldsymbol{b}$ polarization PzR spectra of ReS_2 in the energy range 1.4 to 1.7 eV are respectively shown by the dashed curves in figures 2(a), 2(b) and 2(c). The oscillations on the lower-energy side are caused by the interference effect. The two dominant structures located between 1.54 and 1.6 eV (figure 2(a)) are associated with band-edge excitonic transitions from different origins and were previously assigned as E_1^{ex} and E_2^{ex} [6]. As shown in figure 2(b), the E_2^{ex} feature is absent in $\boldsymbol{E} \perp \boldsymbol{b}$ polarization while the E_1^{ex} feature disappears in $\boldsymbol{E} \perp \boldsymbol{b}$ polarization (see figure 2(c)). In addition, several sharp and prominent features are also detected on the higher-energy side of the spectra of figure 2. From the spectral characteristics of sharp line shape and narrow linewidth of the PzR spectra, these features are most probably originating from the interband excitonic transitions as well. We have fitted the polarized curves to a functional form appropriate for excitonic transitions, that

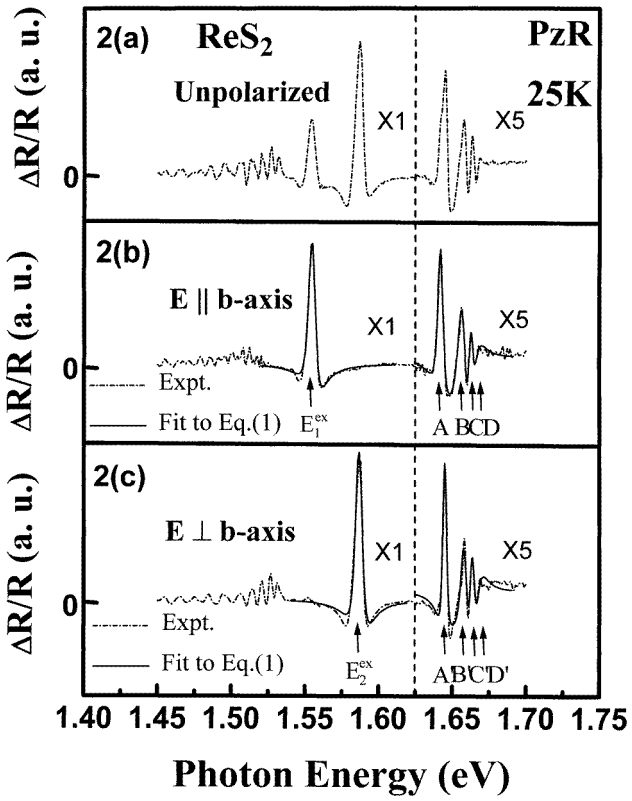

Figure 2. The polarization-dependent PzR spectra (dashed curves) for (a) unpolarized, (b) $\boldsymbol{E} \parallel \boldsymbol{b}$ polarization of and (c) $\boldsymbol{E} \perp \boldsymbol{b}$ polarization of ReS_2 at 25 K. The solid curves are least-squares fits to equation (1), which yield the excitonic transition energies indicated by arrows.

can be expressed as a Lorentzian line-shape function of the form [7, 8]

$$\frac{\Delta R}{R} = \mathrm{Re}\left[\sum_{i=1}^{n} A_i^{ex} \mathrm{e}^{\mathrm{i}\phi_i^{ex}} (E - E_i^{ex} + \mathrm{i}\Gamma_i^{ex})^{-2}\right] \tag{1}$$

where A_i^{ex} and ϕ_i^{ex} are, respectively, the amplitude and phase of the line shape, and E_i^{ex} and Γ_i^{ex} are, respectively, the energy and broadening parameter of the interband excitonic transitions. Shown by the solid curves in figures 2(b) and 2(c) are the least-squares fits obtained using equation (1). The interband excitonic transition energies obtained for the features denoted as E_1^{ex} and A–D (or E_2^{ex} and A′–D′) are summarized in table 1. The locations of the peaks are indicated by arrows at the bottom of figure 2(b) (or figure 2(c)), and the features A–D have a one-to-one correspondence with the features A′–D′. The features with $\boldsymbol{E} \parallel \boldsymbol{b}$ polarization are slightly smaller than those with $\boldsymbol{E} \perp \boldsymbol{b}$ polarization. A multitude of interband excitonic transitions are detected, which is most probably a consequence of triclinic low-symmetry structures of ReS_2. The unpolarized spectrum can be regarded as a random superposition of the spectra with $\boldsymbol{E} \parallel \boldsymbol{b}$ and $\boldsymbol{E} \perp \boldsymbol{b}$ polarization.

Figure 3 shows the polarization-dependent PzR spectra of ReS_2 at room temperature. Only the features E_1^{ex} and A (or E_2^{ex} and A′) are detected at room temperature. The features B, C and D (or B′, C′ and D′) are ionized and become undetectable at room temperature. The solid curves are least-squares fits to equation (1). The energy values obtained are denoted by

Table 1. Excitonic transition energies of ReS_2 which are deduced from the Lorentzian line-shape fits of the PzR spectra at 25 and 300 K.

Feature	Polarization	Transition energy (eV)	Temperature (K)
E_1^{ex}	$\boldsymbol{E} \parallel \boldsymbol{b}$	1.555 ± 0.002	25
A	$\boldsymbol{E} \parallel \boldsymbol{b}$	1.642 ± 0.001	25
B	$\boldsymbol{E} \parallel \boldsymbol{b}$	1.656 ± 0.001	25
C	$\boldsymbol{E} \parallel \boldsymbol{b}$	1.662 ± 0.001	25
D	$\boldsymbol{E} \parallel \boldsymbol{b}$	1.664 ± 0.001	25
E_2^{ex}	$\boldsymbol{E} \perp \boldsymbol{b}$	1.587 ± 0.002	25
A′	$\boldsymbol{E} \perp \boldsymbol{b}$	1.645 ± 0.001	25
B′	$\boldsymbol{E} \perp \boldsymbol{b}$	1.659 ± 0.001	25
C′	$\boldsymbol{E} \perp \boldsymbol{b}$	1.664 ± 0.001	25
D′	$\boldsymbol{E} \perp \boldsymbol{b}$	1.665 ± 0.001	25
E_1^{ex}	$\boldsymbol{E} \parallel \boldsymbol{b}$	1.485 ± 0.005	300
A	$\boldsymbol{E} \parallel \boldsymbol{b}$	1.569 ± 0.005	300
E_2^{ex}	$\boldsymbol{E} \perp \boldsymbol{b}$	1.519 ± 0.005	300
A′	$\boldsymbol{E} \perp \boldsymbol{b}$	1.576 ± 0.005	300

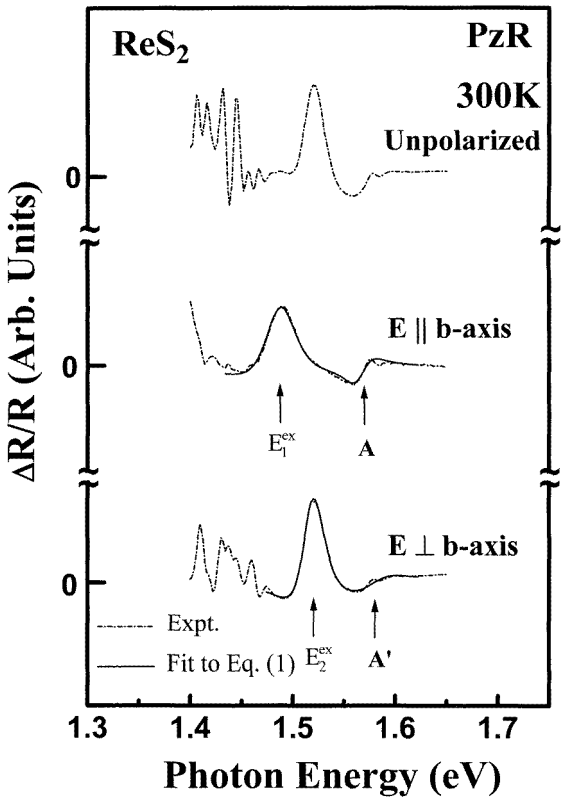

Figure 3. The polarization-dependent PzR spectra of ReS_2 at room temperature.

arrows and listed in table 1 as well. As expected, the excitonic transition energies at room temperature are smaller than those at 25 K. The shifts of the A and A′ features between 25 and 300 K are similar to those of E_1^{ex} and E_2^{ex}. The identical temperature dependence for the

observed transitions for ReS_2 lends additional support to the proposal that the origin of these features is related to the interband excitonic transitions.

Figure 4 displays the absorption coefficient as a function of the photon energy for ReS_2 at 25 and 300 K. The dashed curves in figure 4 correspond to the $\boldsymbol{E} \parallel \boldsymbol{b}$ polarization, the dotted curves represent $\boldsymbol{E} \perp \boldsymbol{b}$ polarization and the solid curves are the unpolarized results. The polarization dependence of the absorption curves provides conclusive evidence that the two optical absorption edges are associated with interband transitions from different origins. The absorption edge shifted toward higher energies as the temperature of the sample was lowered. Analysis of the polarization-dependent experimental data on the absorption coefficient α shows an indirect allowed transition for the material.

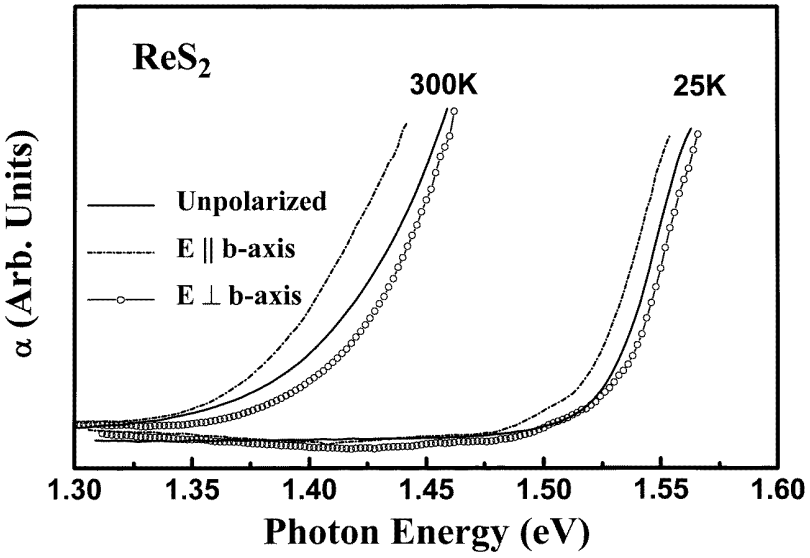

Figure 4. The absorption coefficient as a function of the photon energy for ReS_2 at 25 and 300 K. The dashed curves correspond to the $\boldsymbol{E} \parallel \boldsymbol{b}$ polarization, the dotted curves represent $\boldsymbol{E} \perp \boldsymbol{b}$ polarization and the solid curves are the unpolarized spectra.

The experimental points for $\alpha h\nu$ versus $h\nu$ that are deduced from polarization-dependent absorption measurements for ReS_2 at 25 and 300 K are shown in figure 5. The hollow circles (hollow squares) are data points from the $\boldsymbol{E} \parallel \boldsymbol{b}$ ($\boldsymbol{E} \perp \boldsymbol{b}$) polarization measurements and the solid curves are the least-squares fits to the expression [9]

$$\alpha h\nu = \frac{A(h\nu - E_g + E_p)^2}{\exp(E_p/kT) - 1} + \frac{B(h\nu - E_g - E_p)^2}{1 - \exp(-E_p/kT)} \tag{2}$$

where $h\nu$ is the energy of the incident photon, E_g the band gap, E_p the energy of the phonon assisting the transition, and A and B are constants. The first term on the right-hand side of equation (2) corresponds to an absorption of a photon and a phonon, whereas the second term corresponds to an absorption of a photon and emission of a phonon and contributes only when $h\nu \geqslant E_g + E_p$. There is a large residual absorption at photon energies below the absorption edge. The large values of the absorption coefficient α below the absorption edge of ReS_2 most probably indicate the existence of impurities or defects in the materials. At this point, we have not considered in detail the effect of these impurity or defect states. For simplicity, in our present study, the residual absorption is assumed to be a constant and subtracted out for the

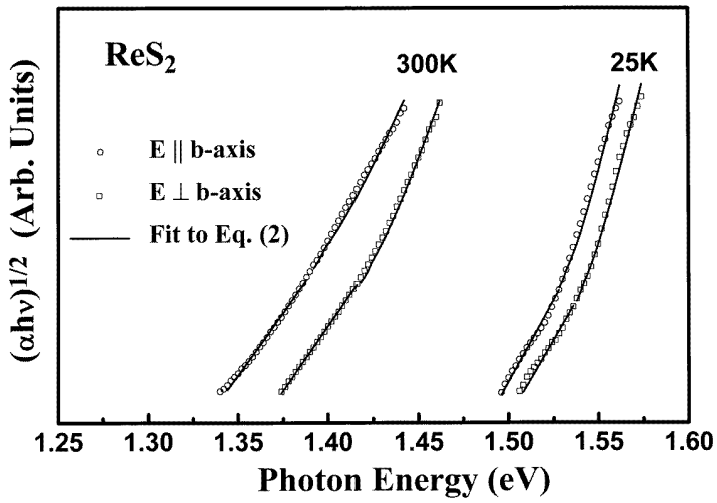

Figure 5. The experimental points for $(\alpha h\nu)^{1/2}$ versus $h\nu$ that are deduced from polarization-dependent absorption measurements for ReS_2 at 25 and 300 K, where the hollow circles (solid squares) are the data points obtained from the $\boldsymbol{E} \parallel \boldsymbol{b}$ ($\boldsymbol{E} \perp \boldsymbol{b}$) polarization measurements and the solid curves are least-squares fits to equation (2).

evaluation of the band gap E_g and phonon energy E_p. The results indicate that ReS_2 is an indirect semiconductor, in which $\boldsymbol{E} \parallel \boldsymbol{b}$ polarization exhibits a smaller band gap and a single phonon makes an important contribution in assisting the indirect transitions. The nonuniform thickness and nonsmooth sample surface will tend to cause the angles of incidence to deviate from the normal direction, resulting in some variations in the absorption spectra. Differing values of E_g and E_p could be obtained by fitting a different energy range; thus errors of the order of ± 0.02 eV and ± 5 meV can be deduced for the estimates of E_g and E_p, respectively. The fitted values of the energy gap and phonon energy of ReS_2 are summarized in table 2. The value of the phonon's energy is 25 ± 5 meV and seems to be insensitive to the temperature. The value of the phonon energy shows that it is not an acoustic phonon but a phonon from one of the numerous optical branches. The optical branches are relatively flat as compared with the acoustic branches and, since the phonon momentum needed for an indirect interband transition is large, agreement of the phonon energies with zone-centre optical phonon energies is not expected.

As shown in table 2, the indirect gaps at 25 and 300 K, denoted as $E_{g\parallel}$ ($E_{g\perp}$), are respectively determined to be 1.51 ± 0.02 eV (1.52 ± 0.02 eV) and 1.35 ± 0.02 eV (1.38 ± 0.02 eV). Here, $E_{g\parallel}$ and $E_{g\perp}$ refer respectively to the indirect gaps for the $\boldsymbol{E} \parallel \boldsymbol{b}$ and $\boldsymbol{E} \perp \boldsymbol{b}$ polarizations. It is noticed that the value of E_g as determined from the absorption data for the unpolarized incident light lies between $E_{g\parallel}$ and $E_{g\perp}$. The origin of the unpolarized

Table 2. The values of the energy gap and phonon energy of ReS_2 which are derived from the analysis of absorption measurements made at 25 and 300 K.

Material	$E_{g\parallel}$ (eV)	$E_{g\perp}$ (eV)	E_p (meV)	Temperature (K)
ReS_2	1.51 ± 0.02	1.52 ± 0.02	22 ± 5	25
ReS_2	1.35 ± 0.02	1.38 ± 0.02	25 ± 5	300

spectra can be regarded as a random superposition of the $\boldsymbol{E} \parallel \boldsymbol{b}$ and $\boldsymbol{E} \perp \boldsymbol{b}$ polarization spectra. Analysis of the absorption spectra reveals that the values of the energy gaps $E_{g\parallel}$ and $E_{g\perp}$ are slightly different to the previous published ones derived from unpolarized measurements [10, 11]. The absorption anisotropy in the van der Waals planes may be a general characteristic of materials with triclinic layered structures.

A study of the electrical anisotropy of ReS_2 along and perpendicular to the *b*-axis was carried out by means of temperature-dependent resistivity measurements over the temperature range 80 to 300 K. For comparison purposes, resistivity measurement along the *c*-axis was also carried out. Figure 6 shows the resistivity of ReS_2 single crystals, where the solid squares, hollow circles and solid diamonds are data points deduced from the resistivity measurements with the electrical fields along the *c*-axis, perpendicular to the *b*-axis and parallel to the *b*-axis, respectively. The results indicate that the $\rho_{\parallel b}$ are smaller than the $\rho_{\perp b}$ and at least three orders of magnitude smaller than the $\rho_{\parallel c}$. $\rho_{\parallel c}$ taking large values is a general electrical property of layer-type crystals, due to the weak van der Waals bonding between individual layers [1]. The smallest values of the resistivity parallel to *b*-axis can mostly be related to the strongest bonding force of ReS_2 which exists along the crystal orientation of the Re-cluster chains.

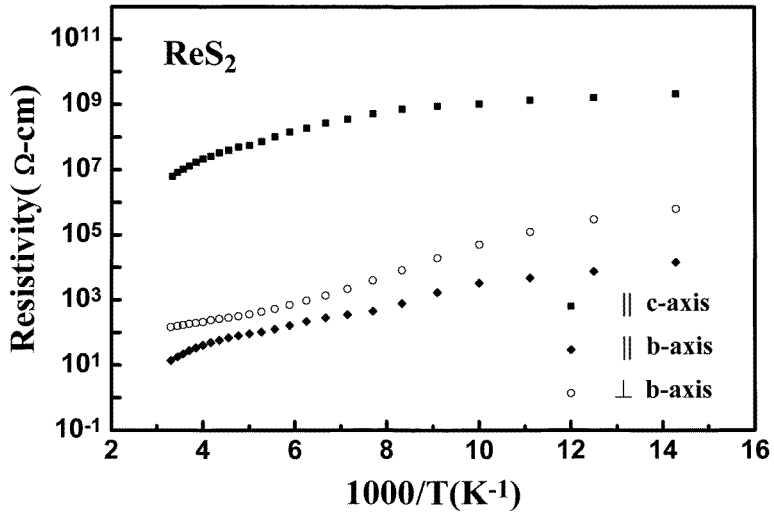

Figure 6. The temperature-dependent resistivity of ReS_2. The solid squares, hollow circles and solid diamonds are data points deduced from the resistivity measurements along the *c*-axis, perpendicular to the *b*-axis and parallel to the *b*-axis, respectively.

4. Summary

In summary, we have studied the in-plane anisotropic optical and electrical properties of ReS_2 crystals. The optical anisotropic effects for $\boldsymbol{E} \parallel \boldsymbol{b}$ polarization and $\boldsymbol{E} \perp \boldsymbol{b}$ polarization are studied through polarization-dependent PzR and optical absorption measurements. The PzR features, which originate from the interband excitonic transitions, with $\boldsymbol{E} \parallel \boldsymbol{b}$ polarization are slightly lower than those with $\boldsymbol{E} \perp \boldsymbol{b}$ polarization. The results of an optical absorption study indicate that $\boldsymbol{E} \parallel \boldsymbol{b}$ polarization exhibits a smaller indirect band gap. The smallest values of the resistivity parallel to the *b*-axis can mostly be related to the strongest bonding force of ReS_2, which exists along the crystal orientation of the Re-cluster chains.

Acknowledgments

C H Ho and Y S Huang acknowledge the support of the National Science Council of the Republic of China under Project No NSC88-2112-M-011-001 and K K Tiong acknowledges the support of the National Science Council of the Republic of China under Project No NSC88-2112-M-019-004.

References

[1] Wilson J A and Yoffe A D 1969 *Adv. Phys.* **18** 193
[2] Wildervanck J C and Jellinek F 1971 *J. Less-Common Met.* **24** 73
[3] Liang W Y 1973 *J. Phys. C: Solid State Phys.* **6** 551
[4] Lamfers H J, Meetsma A, Wiegers G A and de Boer J L 1996 *J. Alloys Compounds* **241** 34
[5] Friemelt K, Lux-Steiner M Ch and Bucher E 1993 *J. Appl. Phys.* **74** 5266
[6] Ho C H, Liao P C, Huang Y S and Tiong K K 1997 *Phys. Rev.* B **55** 25 608
[7] Aspnes D E 1980 *Optical Properties of Semiconductors (Handbook on Semiconductors vol 2)* ed M Balkanski (Amsterdam: North-Holland) p 109
[8] Pollak F H and Shen H 1993 *Mater. Sci. Eng.* R **10** 275
[9] Pankove J I 1975 *Optical Processes in Semiconductors* (New York: Dover)
[10] Marzik J V, Kershaw R, Dwight K and Wold A 1984 *J. Solid State Chem.* **51** 170
[11] Ho C H, Liao P C, Huang Y S, Yang T R and Tiong K K 1997 *J. Appl. Phys.* **81** 6380